Maximum velocity estimation in coronary arteries using 3D tracking Doppler

Stefano Fiorentini*, *Student Member, IEEE*, Lars Mølgaard Saxhaug*, Tore Bjåstad*, Espen Holte*, Hans Torp*, *Member, IEEE*, Jørgen Avdal*, *Member, IEEE*
*Department of Circulation and Medical Imaging, Norwegian University of Science and Technology, Trondheim, Norway
Email: stefano.fiorentini@ntnu.no

***Abstract*—Several challenges currently prevent the use of Doppler echocardiography to assess blood flow in the coronary arteries. Due to the anatomy of the coronary tree, out-of-plane flow and high beam-to-flow angles easily occur. Transit time broadening in regions with high velocities leads to overestimation of the maximum velocity envelope, which is a standard clinical parameter for flow quantification. In this work, a commercial ultrasound system was locally modified to perform trans-thoracic, 3D high frame-rate imaging of the coronary arteries. The imaging sequence was then combined with 3D tracking Doppler for retrospective estimation of maximum velocities. Results from simulations showed that 3D tracking Doppler delivers sonograms with better velocity resolution and spectral SNR compared to conventional PW Doppler. Results were confirmed using *in vitro* recordings. Further simulations based on realistic coronary flow data showed that 3D tracking Doppler can provide improved performance compared to PW Doppler, suggesting a potential benefit on patients. *In vivo* feasibility of the method was also shown in a healthy volunteer.**

I. INTRODUCTION

THE coronary arteries provide oxygen to the cardiac muscles, which are responsible for the pumping function of the heart. In Coronary Artery Disease (CAD), the growth of atherosclerotic plaques causes a decrease in the amount of blood flow to cardiac tissues, impeding the delivery of oxygen and nutrients. The prolonged lack of oxygen can result in chronic or acute heart failure. Coronary artery disease is the first cause of death globally [1].

CAD assessment using ultrasound is an ongoing research field. Stress echocardiography [2] is already part of standard clinical procedures. Myocardial perfusion imaging using contrast agents has been investigated for several years [3]. New methods for coronary microvascular angiography using ultrafast ultrasound imaging have recently been proposed [4], [5]. Trans-thoracic Pulsed Wave (PW) Doppler has also been investigated as a potential candidate for CAD assessment. Several feasibility studies have used PW Doppler to measure coronary flow velocity reserve [6], post-stenotic diastolic-to-systolic velocity ratio [7] or post-stenotic to stenotic velocity ratio [8].

However, the use of trans-thoracic PW Doppler for CAD assessment in the clinics is prevented by several challenges. Beam-to-flow angles above 60° and out-of-plane flow easily occur [9]. Clutter filtering is a challenging task [10], as many cardiac structures move at relatively high velocities. The effective observation time is limited by the ratio between the focal region size and the scatterer velocity. This phenomenon, known as transit time effect, is a source of undesired spectral broadening, which reduces the intra- and inter- observer reproducibility of maximum velocity measurements [11], [12].

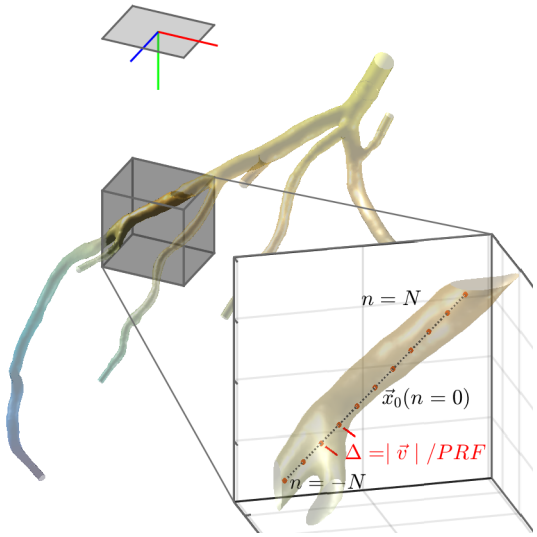

Fig. 1. A 2D matrix ultrasound transducer is used to record the backscattered signal arising from the grey volume. 3D tracking Doppler spectral power is estimated by summing in slow-time pre-envelope data interpolated at the orange points along the tracking direction. The distance between consecutive samples is equal to the distance covered by a scatterer moving at the velocity of interest during the Pulse Repetition Period T = 1 / PRF.

Several velocity estimators have been proposed to address the above mentioned problems [13]–[15]. In the context of coronary flow imaging, spectral estimators might be more suitable than mean velocity estimators, due to the challenge in completely suppressing clutter within the sample volume and to the low spatial resolution available. Studies have shown that adaptive spectral estimators such as the minimum variance Capon estimator [16] and amplitude and phase estimator (APES) [17] provide spectra with increased velocity resolution compared to the conventional Welch estimator [18], but they are less effective when the main cause of broadening is reduced observation time [19].

In 2D tracking Doppler, a broad-band method developed by Fredriksen et al. [20], plane wave imaging is used to track the scatterers along straight trajectories in the imaging plane.

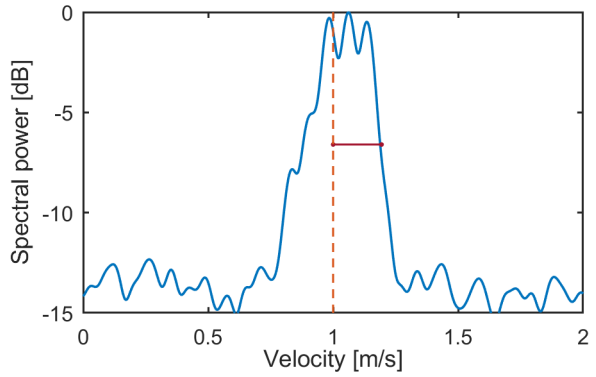

Fig. 2. Illustration of the method to measure velocity overestimation. Velocity overestimation is defined as the difference between the maximum velocity and the ground truth velocity, having assumed a uniform velocity profile in the phantoms. The maximum velocity is evaluated at -6 dB below the spectral power at the ground truth velocity. To account for variance, the power at ground truth velocity is averaged in an interval equal to $\pm 2\%$ of the Nyquist limit.

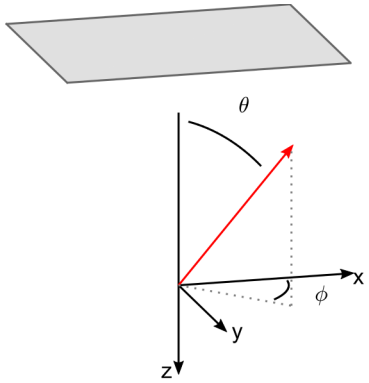

Fig. 3. Spherical coordinate system used to define rotations. ϕ is the axial rotation angle and θ is the beam-to-flow angle.

Pre-envelope samples are summed along skewed lines in the fast-slow time matrix, with slope corresponding to the axial velocity that is being estimated. The result is a complete velocity spectrum with reduced transit time broadening and increased SNR compared to conventional PW Doppler. The method was tested on vascular imaging, but the expected improvement in velocity resolution and spectral SNR make it a promising candidate for coronary flow imaging as well. However, as only the in-plane velocity component is evaluated, velocity underestimation is expected in coronary imaging because it is difficult to avoid out-of-plane flow. This limitation motivates a further extension of the method to 3D.

In this work, we combine a non-compounded, 3D plane wave imaging sequence with a 3D extension of the tracking Doppler method to provide a framework for retrospective estimation of velocity spectra in the coronary arteries. By coherently summing IQ data sampled along a straight line, 3D tracking Doppler is expected to follow the scatterers over a longer observation window compared to conventional PW Doppler, therefore reducing transit time broadening and increasing the accuracy of maximum velocity measurements. The imaging sequence is implemented on a locally modified commercial ultrasound system equipped with a trans-thoracic 2D matrix array probe. This work is an extension of a previous conference paper [21].The theoretical framework behind 3D tracking Doppler is described in section II. *In silico*, *in vitro* and *in vivo* studies are described in section III. The results are shown in section IV and discussed in section V.

II. 3D Tracking Doppler Algorithm

In our proposed algorithm, a full velocity spectrum is estimated from a complex-envelope 3D + time dataset $s_{IQ}(\vec{r}, k)$, where $\vec{r} = [x, y, z]$ denotes the spatial coordinates and k is the frame index. The temporal distance between consecutive frames is equal to the Pulse Repetition Period and is denoted throughout this section as T. The spectral estimation process is accomplished in two steps.

For every velocity v of interest, a packet of $2N+1$ points is sampled in space along a straight trajectory using 3D interpolation. The procedure is performed for every frame. The samples are symmetric to a prescribed coordinate $\vec{x}_0 = [x_0, y_0, z_0]$, with $\Delta = vT$ spacing, as depicted in Figure 1. The resulting signal is a function of distance along the tracking direction and slow time, and can be considered as a pseudo M-Mode matrix. A new pseudo M-Mode matrix is generated for every velocity of interest.

The spectral power $\hat{P}(v, k)$ is estimated by squaring the sum of samples within each packet. This operation is equal to squaring the sum of elements in the pseudo M-Mode matrix along the diagonals

$$\hat{P}(v,k) = \left| \sum_{n=-N}^{N} w(n)\hat{s}(\vec{x}_0 + nT\vec{v}, k+n) \right|^2 \tag{1}$$

where $\vec{v}$ is a three dimensional vector that defines the tracking direction and whose magnitude is equal to the tracking velocity, $n \in [-N, N]$ is the sample index within a packet and $2N+1$ is the packet size. A window function $w(n)$ of length $2N+1$ is applied to reduce side lobes in the spectrum. Using an odd window length ensures that the packet is centred at $\vec{x}_0$. In order to apply the algorithm on IQ data, a phase correction term must be applied before summation to account for radial motion

$$\hat{s}(\vec{r}, k) = s_{IQ}(\vec{r}, k) e^{i2\pi f_d \vec{r}\cdot\vec{a}} \tag{2}$$

where f_d is the demodulation frequency and $\vec{a}$ is a unit vector that defines the direction of the transmit beam. Therefore, $\vec{r}\cdot\vec{a}$ is the projection of the sample coordinates on the direction of the transmit beam. The PW Doppler spectral power estimate P at $\vec{x}_0$ is given by

$$P(v,k) = \left| \sum_{n=-N}^{N} w(n) s_{IQ}(\vec{x}_0, k+n) e^{i2\pi \bar{f} n \Delta t} \right|^2 \tag{3}$$

Attenuation in the medium causes a shift in the center frequency of the received signal $\bar{f}$, which can result in a difference between $\bar{f}$ and f_d.

TABLE I
IN VITRO, IN SILICO AND IN VIVO SETUP PARAMETERS

IN VITRO - IN SILICO				IN VIVO			
ACQUISITION		POST PROCESSING		ACQUISITION		PROCESSING	
Parameter	Value	Parameter	Value	Parameter	Value	Parameter	Value
Tx frequency f0	3.1 [MHz]	Clutter filter	Butterworth 10	Tx frequency f0	3.1 [MHz]	Clutter filter	Butterworth 10
PRF	6.5 [kHz]	Cutoff	150 [Hz]	PRF	4.5 [kHz]	Cutoff	250 [Hz]
Pulse cycles at f0	3.5	Window size	65	Pulse cycles at f0	3.5	Window size	135
IQ sampling freq. fs	4 [MHz]	Window	Hamming	IQ sampling freq. fs	4 [MHz]	Window	Hamming
Demodulation freq. fd	2.9 [MHz]	Tracking length	15 [mm]	Demodulation freq. fd	2.9 [MHz]	Tracking length	15 [mm]

III. METHODS

A. Performance assessment

We investigated the sensitivity of 3D tracking Doppler performance to vessel orientation, tracking direction and imaging depth. The study was based on synthetic RF channel data generated in MATLAB using Field II [22], [23]. RF sampling frequency was set as high as 100 MHz to avoid aliasing. GE 4V transducer's geometry (20.6 mm azimuth aperture, 16.5 mm elevation aperture, 0.343 mm pitch, 60 azimuth elements, 48 elevation elements) and impulse response were used. Sub Aperture Processing was not simulated. The phantom consisted of a rigid cylinder filled with randomly generated point scatterers with a density of 10 scatterers per resolution cell. A 1 m/s uniform velocity profile was prescribed over the cross section of the cylinder. The phantom was imaged using a non-compounded plane wave sequence. Frequency dependent attenuation was not taken into consideration. Synthetic RF channel data were band-pass filtered, complex demodulated and decimated. Channel data were beamformed with a conventional delay-and-sum algorithm and expanding aperture with hamming apodization. White Gaussian noise was added to beamformed data to achieve a 20 dB SNR in PW Doppler sonograms. Clutter filtering was also performed before spectral estimation, using the filter specifications in Table I. PW Doppler and 3D tracking Doppler spectra were estimated from the same dataset according to equations (3) and (1), using a 65 samples Hamming window. Spectra were averaged over 20 ms in slow time. PW spectra were also averaged over a 3 mm range span while 3D tracking Doppler spectra were averaged along the tracking direction. The maximum tracking length was limited to 15 mm. The acquisition and post processing parameters are given in Table I.

We used the maximum velocity overestimation as a measure of performance for both 3D tracking Doppler and PW Doppler. The maximum velocity overestimation was measured as the difference between the true maximum velocity and the velocity corresponding to the -6 dB value below the signal power averaged around the true maximum. An example is given in Figure 2. The sensitivity of velocity overestimation to three parameters was investigated.

1) Vessel orientation: The phantom was placed at 40 mm depth and was rotated from the reference position according to the spherical coordinate system in Figure 3. To reduce the total number of simulations needed for a complete characterization, we exploited the symmetry of the transducer's geometry about its two main axes. The radial rotation angle ϕ spanned the range $[0°, 90°]$ with $15°$ steps, while the beam to flow angle θ spanned the range $[15°, 75°]$ with $15°$ steps. PW Doppler and 3D tracking Doppler spectra were estimated using the correct tracking direction and angle correction.

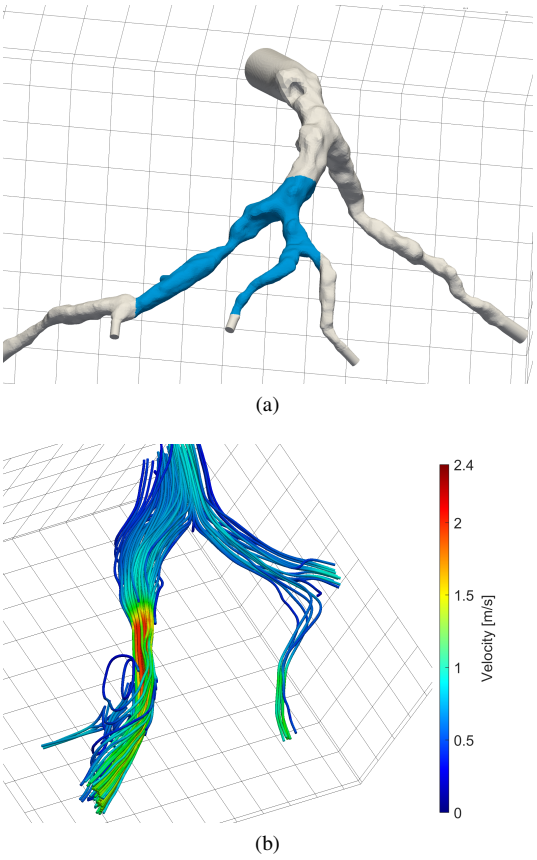

(a)

(b)

Fig. 4. The geometry of a stenotic left coronary artery is shown in (a). The portion of the velocity field used in the ultrasound simulation is highlighted in blue and a red circle highlights the stenotic region. The velocity field at the stenosis is depicted in (b) using streamlines. The maximum velocity magnitude is 2.4 m/s.

2) Tracking direction: The phantom was placed at 40 mm depth and oriented at $[\phi = 45°, \theta = 75°]$ according to the adopted coordinate system in Figure 3. Several tracking Doppler spectra were generated from the same dataset by rotating the correct tracking direction with $[\Delta\phi, \Delta\theta]$ angles. All combinations of $\Delta\phi$ and $\Delta\theta$ in the range $[-5°, 5°]$ with $1°$ steps were considered.

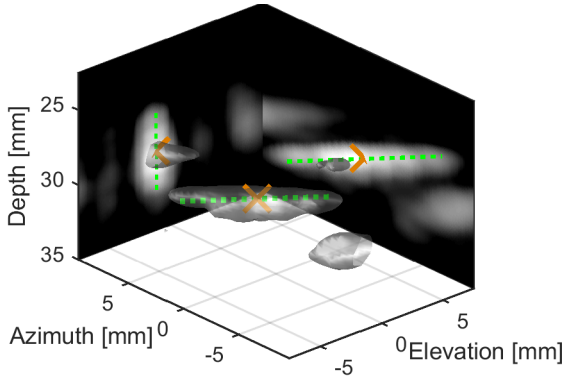

Fig. 5. 3D power Doppler and projection planes used for manual selection of PW sample volume and tracking Doppler segment. The tracking direction was chosen based on the projection planes and validated using the 3D power Doppler rendering. The tracking segment is shown in green, and PW sample volume is shown with an orange marker.

3) Imaging depth: The phantom was placed at increasing depth, from 30 mm to 100 mm with 10 mm increments. Two different beam to flow angles, $\theta = 75°$ and $\theta = 60°$, were considered. 3D tracking Doppler spectra were estimated along the true flow direction.

B. Simulation based on a realistic velocity field

We compared PW Doppler and 3D tracking Doppler power spectra on a synthetic dataset based on a realistic velocity field, that was generated using the framework described by Swillens et al. [24]. The coronary tree of a patient with a stenotic Left Anterior Descending (LAD) coronary artery was manually segmented from an angio-CT scan using the Vascular Modeling Toolkit (VMTK) [25]. The geometry was used as input to the Computational Fluid Dynamics (CFD) software Fenics [26], [27]. A steady state solution was obtained by running a time-dependent solver with constant pressure at the inlet and constant resistance at the outlets. The solution was propagated in time until the stationarity condition was attained. The resistance values at the outlets were set to reproduce the effects of hyperaemia. The pressure field from the solution was also able to reproduce to some extent invasive Fractional Flow Reserve (FFR) measurements performed on the patient. The velocity field from the solution, shown in Figure 4b, was used to propagate scatterers in a Field II simulation. The vessel geometry was filled with randomly generated scatterers with a density of 75 scatterers per resolution cell. The higher density value than in section III-A was determined heuristically to reduce variance in velocity distribution due to the random placement of the scatterers inside the phantom. The Field simulation time span was set to 20 ms, to ensure the fulfilment of the stationarity condition. The phantom was imaged using a non-compounded plane wave sequence. The post-processing framework was the same as described in section III-A. The acquisition and post processing parameters are given in Table I. Both PW Doppler and 3D tracking Doppler spectra were estimated from the same dataset. PW Doppler was averaged along the range direction while no spatial averaging was performed for 3D tracking Doppler.

C. In vitro validation

In vitro flow data were recorded from a JJ&A Doppler thread phantom (JJ&A instruments, Seattle, United States), programmed to reproduce a pulsatile flow pattern. The thread consisted of an o-ring with 2mm cross-sectional diameter. The recordings were performed on a GE Vivid E95 scanner equipped with a GE 4V matrix cardiac probe (GE Vingmed, Horten, Norway). The ultrasound scanner was locally modified to enable a non-compounded plane wave imaging sequence, which was used to record the phantom. The acquisition parameters are given in Table I. RF channel data were band-pass filtered, complex demodulated and decimated in the scanner. Offline beamforming was performed in MATLAB (2017a, The MathWorks, Natick, United States) using a pixel-based delay and sum (DAS) algorithm and expanding aperture with Hamming apodization. White Gaussian noise was added to beamformed data to achieve a 20 dB SNR in PW Doppler sonograms. Clutter filtering was also performed before spectral estimation, using the filter specifications in Table I. The PW sample volume and the tracking segment were manually chosen after visual inspection of power Doppler. Navigation was limited to azimuth and elevation projections planes for increased robustness, and a 3D rendering was used for a later validation as shown in Figure 5. PW Doppler and tracking Doppler spectra were estimated using equations (3) and (1), with a 65 samples Hamming window. Spectra were averaged over 20 ms in slow time. PW spectra were also averaged over a 3 mm range span whereas tracking Doppler spectra were averaged along the tracking direction. The maximum tracking length was limited to 15 mm.

D. In vivo feasibility

In vivo feasibility of the method and the acquisition setup were investigated on a healthy volunteer. Navigation was performed by a cardiologist using a conventional, focused 2D duplex sequence. The investigated region was the distal part of the LAD coronary artery. The cardiologist adopted a modified two-chamber view and investigated the region until Color Flow could reveal the artery consistently for a few cardiac cycles. The 2D duplex sequence was then paused to enable 1.5 seconds of contiguous non-compounded plane wave acquisition. The dataset was used to estimate 3D Color Flow, PW Doppler and 3D tracking Doppler. During the high-frame rate sequence, the scanner reported a MI of 0.4 and a TI of 1.7. The post-processing workflow described in section III-C was used. Acquisition and post-processing parameters are given in Table I.

IV. Results

A. Performance assessment

In Figure 6, velocity overestimation at -6 dB for 3D tracking Doppler and PW Doppler from synthetic plug flow datasets are compared in a range of beam-to-flow angles θ and axial rotation angles ϕ. Results from same beam-to-flow angle θ (i.e. 7 simulations with axial rotation angle spanning the range $[0°, 90°]$) are grouped together and the standard deviation of

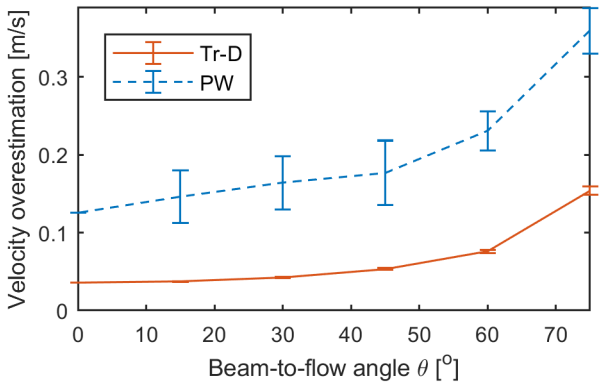

Fig. 6. Velocity overestimation for 3D tracking Doppler and conventional PW Doppler as a function of the beam-to-flow angle. The error bars indicate the standard deviation of the measurements with the axial rotation angle. The true velocity was 1 m/s.

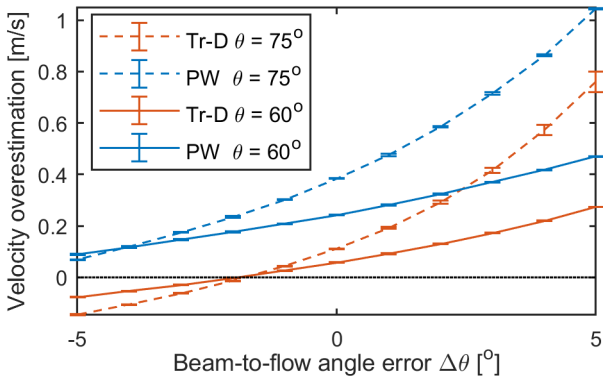

Fig. 7. Velocity overestimation at -6 dB for 3D tracking Doppler (orange) and PW Doppler (blue) as a function of the error in the beam-to-flow angle $\Delta\theta$. The true velocity was 1 m/s, 60° (solid line) and 75° (dashed line) beam-to-flow angles were considered. The error bars indicate the variability in the estimates as a function of the axial rotation angle error$\Delta\phi$.

each group is shown using error bars. A smaller overestimation value means that the maximum velocity envelope is closer to the true maximum velocity. It can be noticed that tracking Doppler consistently delivers higher velocity resolution compared to PW Doppler.

In Figure 7, velocity overestimation at -6 dB for both 3D tracking Doppler and PW Doppler is displayed as a function of the beam-to-flow angle error $\Delta\theta$. 60° and 75° beam-to-flow angles were considered. The standard deviation as a function of the azimuth angle error $\Delta\phi$ is shown using error bars. Small standard deviations suggest that errors in the azimuth angle $\Delta\phi$ do not influence the spectral bandwidth as much as comparable errors in the beam-to-flow angle $\Delta\theta$. Results also show that the estimator is more sensitive to errors as the beam-to-flow angle increases.

In Figure 8, the -6 dB velocity overestimation for 3D tracking Doppler is displayed as a function of imaging depth, at 60° and 75° beam-to-flow angles. Velocity overestimation appears to be not sensitive to imaging depth both at 60° and at 75° up to 9 cm.

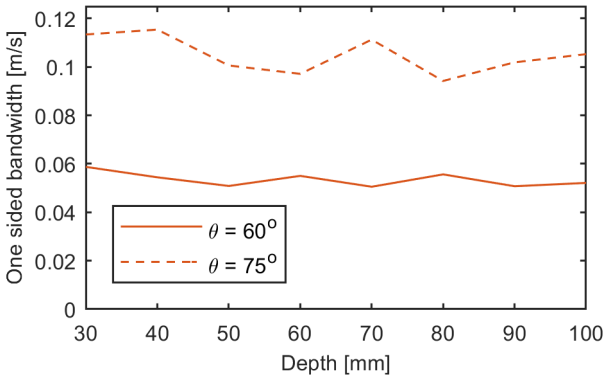

Fig. 8. Velocity overestimation at -6 dB shown as a function of imaging depth, at 60° (blue) and 75° (dashed orange) beam-to-flow angles. The true velocity was 1 m/s.

B. Simulation from a realistic velocity field

PW Doppler, 2D tracking Doppler and 3D tracking Doppler spectra from a realistic velocity field are compared in Figure 9. The maximum velocity magnitude from the CFD simulation is 1.05 m/s and the beam-to-flow angle is 72°. The estimated -6 dB velocity overestimation is 13% for 3D Tracking Doppler and 20% for conventional PW Doppler. 3D tracking Doppler also shows a 3 dB increase in spectral SNR.

C. In vitro validation

3D tracking Doppler and PW Doppler velocity spectra from an *in vitro* recording are compared in Figure 10. The beam-to-flow angle, estimated from visual inspection of power Doppler, was 70°. It is possible to notice ripples in the 3D tracking Doppler spectrum, which are probably caused by vibrations of the thread. The ripples are not visible in the PW Doppler spectrum. In Figure 10b the spectral power corresponding to the white vertical lines in Figure 10a are shown and compared to *in silico* results. The velocity overestimation at -6 dB is approximately 12% for 3D tracking Doppler and 34% for PW Doppler around 1 m/s thread velocity, which is consistent with the simulated results from Figure 6. Results also show a 5 dB spectral SNR increase in 3D tracking Doppler compared to PW Doppler.

D. In vivo feasibility

An *in vivo* 3D CFI rendering of the distal portion of the LAD coronary artery from a healthy volunteer is shown in Figure 11a. 3D color flow was obtained from a contiguous plane wave acquisition using a conventional autocorrelation method. Each autocorrelation estimate was averaged over a 30 ms window. The rendering was obtained by segmenting the surface in which the power of the autocorrelation function matched a manually selected value. The surface is then used as a mask for the corresponding mean velocity estimates. PW Doppler and 3D tracking Doppler sonograms in Figure 11b were estimated retrospectively using the sample volume and tracking direction shown in Figure 11a. The beam-to-flow angle was approximately 60°. Results also show an improvement in spectral resolution around $t = 0.7s$.

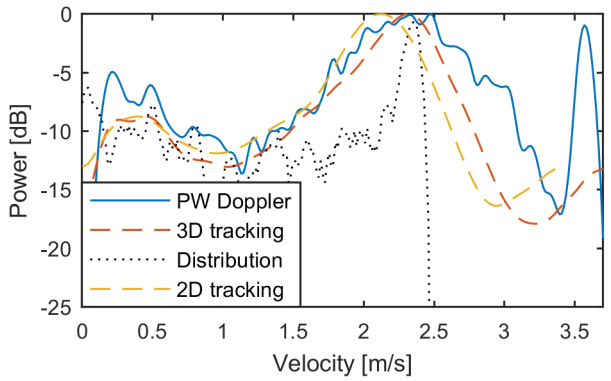

Fig. 9. Spectral power estimates from synthetic data based on a realistic CFD simulation of a stenotic coronary artery. PW Doppler velocity spectrum is shown in solid blue, and 3D tracking Doppler velocity spectrum is shown in dashed orange. 2D tracking Doppler velocity spectrum, shown in dashed yellow, is generated using the same 3D implementation and limiting the tracking direction in the azimuth plane. The underlying velocity distribution is shown in black. The maximum velocity was 2.4 m/s, and the beam to flow angle was 62°.

V. Discussion

In this work we have proposed a 3D extension of the tracking Doppler spectral estimator and have investigated its potential for maximum velocity estimation in the coronary arteries.

Results from Figure 6 show that 3D tracking Doppler consistently provides reduced velocity overestimation compared to a conventional Welch estimator. The small extension of the error bars for 3D tracking Doppler means that the method is not sensitive to the orientation of the flow with respect to the transducer's geometry. This is an important property, considering that coronary arteries can take a variety of spatial orientations within the imaging volume, depending on the patient and the view. As the Welch spectral power was estimated at a fixed spatial location and spatial averaging was performed along the radial direction, the method is expected to be sensitive to the beam-to-flow angle only. Therefore, the measured variability with the axial rotation angle can be interpreted as a variance of the estimator.

Results in Figure 7 show that both tracking Doppler and PW Doppler are sensitive to errors in the beam-to-flow angles. However, a 3° error at 75° beam-to-flow angle in 3D tracking Doppler leads to a velocity overestimation that is comparable to a 3° error at 60° beam-to-flow angle in PW Doppler, indicating that the use of 3D tracking Doppler may increase the range of acceptable beam-to-flow angles.

Results in Figure 8 show that 3D tracking Doppler is not too sensitive to imaging depth, even at high beam-to-flow angles ($\geq 75°$). This a positive quality, considering that coronary arteries can be imaged in a broad range of depths, depending on the branch and the view.

Results from Figure 9 show that 3D tracking Doppler produces sonograms with reduced broadening and increased SNR than conventional PW Doppler even for realistic flow fields, suggesting that the method can potentially improve maximum velocity measurements in patients. However, the improvement

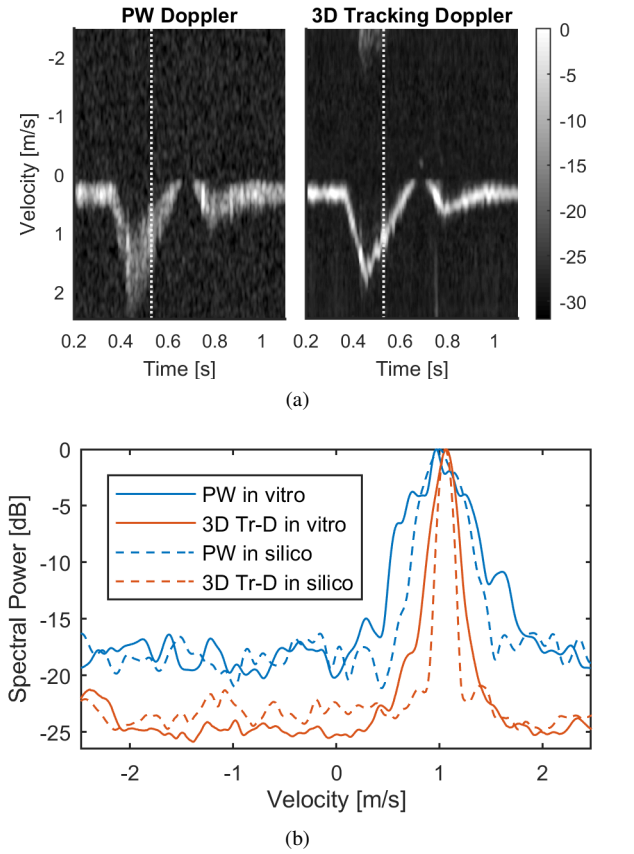

Fig. 10. PW Doppler and 3D tracking Doppler spectral estimates from a thread phantom reproducing a pulsatile flow pattern. The beam-to-flow angle was approximately 70°. In the lower panel, PW Doppler and tracking Doppler spectra corresponding to the white lines in the upper panel are shown and compared to simulated data.

is less pronounced than the ideal plug flow case. In fact, the tracking Doppler method implicitly assumes the signal to be stationary both in time and in space and the assumption is violated along a stenosis, where velocity gradients occur. Although the stationarity assumption in the simulation remains a limiting factor, *in vivo* results in Figure 11b show that blood flow in the left coronary branch is almost constant in mid diastole and that running a stationary simulation over 20 ms is reasonable. Results also show the benefits of a 3D implementation over 2D when out-of-plane flow occurs. In fact, a 2D implementation not only underestimates the maximum velocity, but also shows increased broadening because only the in-plane component can be tracked.

In vitro results in Figure 10b show increased broadening compared to simulations. This may be explained by having averaged the *in vitro* spectrum over a time span in which the stationarity condition is not fulfilled, while the *in silico* spectrum is estimated from a stationary simulation. Results in Figure 10a show that even though 3D tracking Doppler provides higher velocity resolution than PW Doppler at low velocities, the difference between the methods is less significant than at high velocities. This occurs because at low velocities the length of the tracking segment becomes comparable with the spatial extent of the point spread function, leading to only a small increase in observation time.

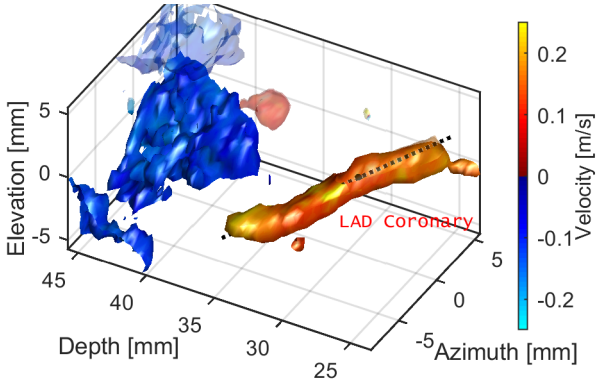

(a)

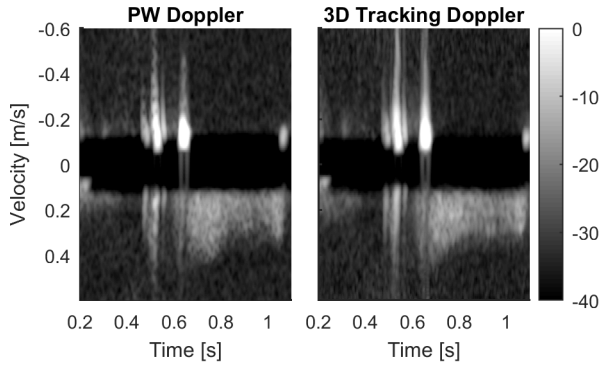

(b)

Fig. 11. *In vivo* recording from a healthy volunteer. A 3D color flow rendering of the left anterior descending (LAD) coronary artery is shown in the upper panel. In the lower panel PW Doppler and 3D tracking Doppler spectral power estimates are compared. The beam-to-flow angle was 60°.

In vivo results from a healthy volunteer show that non-compounded 3D high frame-rate sequences are suitable for trans-thoracic coronary flow imaging and spectral estimation. The maximum investigated depth was 5 cm. Several branches of the coronary tree are located deeper in the chest, motivating further feasibility investigation.

Several reasons could explain why *in vivo* results do not agree with *in vitro* and *in silico* data. First, the reported maximum velocity in the LAD coronary artery of a healthy individual is 0.3 - 0.4 m/s. This value is rather low for 3D tracking Doppler to provide any substantial benefit because the tracking length becomes comparable with the size of the PW sample volume. Increasing the window size is a possible solution, but the time span in which the signal is stationary sets an upper boundary. However, we expect 3D tracking Doppler to perform better at high velocities, as suggested by CFD results. Second, the average size of a coronary artery is comparable to or smaller than the resolution achievable with a cardiac probe. This implies that there will be velocity gradients within the sample volume, along the radius of the vessel and possibly along the axis as well. As previously stated for the CFD phantom, violating the stationarity assumption leads to increased spectral broadening. Finally, relevant parameters for spectral estimation, such as the beam-to-flow angle and the sample volume position, are not updated during the cardiac cycle to compensate for wall motion. This limitation will cause increased spectral broadening at time frames far from the one in which the parameters were chosen.

Being a wideband estimator, 3D tracking Doppler benefits from adopting high pulse frequencies and large apertures, but the choice of parameters is rather limited in coronary applications. The choice is further restricted by the need to use unfocused beams, which reduces both penetration and lateral resolution.

Finally, to ensure that results from PW Doppler and 3D tracking Doppler are comparable, the same acquisition is used for both methods. This benefit may come at the cost of reduced performance for conventional PW Doppler. In fact, the use of unfocused beams may hinder spectral SNR in conventional PW Doppler. On the other hand, reduced lateral resolution can also increase observation time, especially at high beam-to-flow angles, thus reducing transit time broadening. Moreover, as 3D tracking Doppler is a wide-band estimator while conventional PW Doppler is not, the use of a broad-band pulses will benefit the former and impair the latter.

Future work will investigate methods for dynamic tracking direction detection, for example by segmenting the vessel geometry from power Doppler or by combining 3D tracking Doppler with vector Doppler or speckle tracking. Further research is also motivated by reducing the maximum window size to ensure temporal and spatial stationarity without compromising velocity resolution. A possible solution could be to combine 3D tracking Doppler with data dependent spectral estimators [16], [17], as previously done with 2D tracking Doppler for vascular applications [28].

VI. Conclusion

A non-compounded high frame-frame imaging sequence was combined with a 3D extension of the tracking Doppler method to enable retrospective spectral estimation in the coronary arteries. *In vitro* and *in silico* results show that 3D tracking Doppler consistently delivers sonograms with reduced maximum velocity overestimation and increased spectral SNR compared to conventional PW Doppler. Results from simulation also show that 3D tracking Doppler performance is acceptable up to 10 cm depth and 75° beam-to-flow angle. Results from simulations based on realistic coronary flow data suggest that the method can improve the accuracy of maximum velocity measurements in patients. *In vivo* feasibility of the method has also been shown in a healthy volunteer.

VII. Acknowledgement

We would like to thank Lucas Omar Muller at the IVT deparment (NTNU) for providing the CFD phantom.

References

[1] R. Lozano, M. Naghavi, K. Foreman, *et al.*, “Global and regional mortality from 235 causes of death for 20 age groups in 1990 and 2010: A systematic analysis for the global burden of disease study 2010”, *Lancet*, vol. 380, no. 9859, pp. 2095–128, 2012.

[2] R. Sicari and L. Cortigiani, "The clinical use of stress echocardiography in ischemic heart disease", *Cardiovascular Ultrasound*, vol. 15, no. 1, p. 7, 2017.

[3] T. R. Porter and F. Xie, "Myocardial perfusion imaging with contrast ultrasound", *JACC: Cardiovascular Imaging*, vol. 3, no. 2, pp. 176–187, 2010.

[4] D. Maresca, M. Correia, O. Villemain, *et al.*, "Noninvasive imaging of the coronary vasculature using ultrafast ultrasound", *JACC: Cardiovascular Imaging*, p. 2343, 2017.

[5] M. Correia, D. Maresca, J. Provost, *et al.*, "Three-dimensional mapping of epicardial and intramyocardial coronary circulation in-vivo using 3-D ultrafast ultrasound Doppler imaging", in *2017 IEEE International Ultrasonics Symposium (IUS)*, pp. 1–1.

[6] J. Vegsundvåg, E. Holte, R. Wiseth, *et al.*, "Coronary Flow Velocity Reserve in the three main coronary arteries assessed with transthoracic Doppler: A comparative study with quantitative coronary angiography", *Journal of the American Society of Echocardiography*, vol. 24, no. 7, pp. 758–767, 2011.

[7] E. Holte, J. Vegsundvåg, K. Hegbom, *et al.*, "Transthoracic Doppler echocardiography for detection of stenoses in the left coronary artery by use of post-stenotic coronary flow profiles: A comparison with quantitative coronary angiography and Coronary Flow Reserve", *Journal of the American Society of Echocardiography*, vol. 26, no. 1, pp. 77–85, 2013.

[8] E. Holte, J. Vegsundvåg, K. Hegbom, *et al.*, "Transthoracic Doppler for detection of stenoses in the three main coronary arteries by use of stenotic to prestenotic velocity ratio and aliased coronary flow", *European Heart Journal - Cardiovascular Imaging*, vol. 16, no. 12, pp. 1323–1330, 2015.

[9] M. A. Quinones, C. M. Otto, M. Stoddard, *et al.*, "Recommendations for quantification of Doppler echocardiography: A report from the Doppler quantification task force of the Nomenclature and Standards Committee of the American Society of Echocardiography", *J Am Soc Echocardiogr*, vol. 15, no. 2, pp. 167–84, 2002.

[10] A. Yu and L. Lovstakken, "Eigen-based clutter filter design for ultrasound color flow imaging: A review", *IEEE Trans Ultrason Ferroelectr Freq Control*, vol. 57, no. 5, pp. 1096–111, 2010.

[11] V. Newhouse, P. Bendick, and L. Varner, "Analysis of transit time effects on Doppler flow measurement", *IEEE Trans Biomed Eng*, vol. 23, no. 5, pp. 381–6, 1976.

[12] V. Newhouse, E. Furgason, G. Johnson, and D. Wolf, "The dependence of ultrasound Doppler bandwidth on beam geometry", *IEEE Transactions on Sonics and Ultrasonics*, vol. 27, no. 2, pp. 50–59, 1980.

[13] O. Bonnefous and P. Pesque, "Time domain formulation of pulse-Doppler ultrasound and blood velocity estimation by cross correlation", *Ultrason Imaging*, vol. 8, no. 2, pp. 73–85, 1986.

[14] J. A. Jensen and S. I. Nikolov, "Directional synthetic aperture flow imaging", *IEEE Trans Ultrason Ferroelectr Freq Control*, vol. 51, no. 9, pp. 1107–18, 2004.

[15] C. A. Villagómez-Hoyos, S. Holbek, M. B. Stuart, and J. A. Jensen, "High frame rate synthetic aperture 3D vector flow imaging", in *Ultrasonics Symposium (IUS), 2016 IEEE International*, IEEE, pp. 1–4.

[16] J. Capon, "High-resolution frequency-wavenumber spectrum analysis", *Proceedings of the IEEE*, vol. 57, no. 8, pp. 1408–1418, 1969.

[17] J. Li and P. Stoica, "An adaptive filtering approach to spectral estimation and SAR imaging", *IEEE Transactions on Signal Processing*, vol. 44, no. 6, pp. 1469–1484, 1996.

[18] F. Gran, A. Jakobsson, and J. A. Jensen, "Adaptive spectral Doppler estimation", *IEEE Trans Ultrason Ferroelectr Freq Control*, vol. 56, no. 4, pp. 700–14, 2009.

[19] I. K. Ekroll, H. Torp, and L. Lovstakken, "Spectral Doppler estimation utilizing 2-D spatial information and adaptive signal processing", *IEEE Trans Ultrason Ferroelectr Freq Control*, vol. 59, no. 6, pp. 1182–92, 2012.

[20] T. D. Fredriksen, I. K. Ekroll, L. Lovstakken, and H. Torp, "2-D tracking Doppler: A new method to limit spectral broadening in pulsed wave Doppler", *IEEE Trans Ultrason Ferroelectr Freq Control*, vol. 60, no. 9, pp. 1896–905, 2013.

[21] S. Fiorentini, L. Saxhaug, T. Bjåstad, *et al.*, "3D tracking Doppler for quantitative blood flow assessment of coronary arteries", in *2017 IEEE International Ultrasonics Symposium (IUS)*, pp. 1–1.

[22] J. A. Jensen and N. B. Svendsen, "Calculation of pressure fields from arbitrarily shaped, apodized, and excited ultrasound transducers", *IEEE Trans Ultrason Ferroelectr Freq Control*, vol. 39, no. 2, pp. 262–7, 1992.

[23] J. A. Jensen, "Field: A program for simulating Ultrasound systems", *Medical & Biological Engineering & Computing*, vol. 34, pp. 351–353, 1996.

[24] A. Swillens, L. Lovstakken, J. Kips, *et al.*, "Ultrasound simulation of complex flow velocity fields based on Computational Fluid Dynamics", *IEEE Trans Ultrason Ferroelectr Freq Control*, vol. 56, no. 3, pp. 546–56, 2009.

[25] L. Antiga, M. Piccinelli, L. Botti, *et al.*, "An image-based modeling framework for patient-specific computational hemodynamics", *Med Biol Eng Comput*, vol. 46, no. 11, pp. 1097–112, 2008.

[26] A. Logg, K.-A. Mardal, and G. Wells, *Automated solution of differential equations by the finite element method: The FEniCS book*. Springer Science & Business Media, 2012, vol. 84.

[27] M. Alnæs, J. Blechta, J. Hake, *et al.*, "The FEniCS project version 1.5", *Archive of Numerical Software*, vol. 3, no. 100, pp. 9–23, 2015.

[28] Y. Karabiyik, J. Avdal, I. K. Ekroll, *et al.*, "Data adaptive 2-D tracking Doppler", in *2016 IEEE International Ultrasonics Symposium (IUS)*.